Journal of Alloys and Compounds 1012 (2025) 178436

Contents lists available at ScienceDirect

Journal of Alloys and Compounds

journal homepage: www.elsevier.com/locate/jalcom

High performance soft magnetic composites based on Fe/Ni-Zn ferrite powder prepared by low-pressure spark plasma sintering

Changgeng Zhang [a,b], Ziran Guo [a,b], Zhiwei Lin [a,b,c,*], Yongjian Li [a,b]

[a] State Key Laboratory of Reliability and Intelligence of Electrical Equipment, Hebei University of Technology, Tianjin 300401, PR China
[b] Hebei Key Laboratory of Equipment and Technology Demonstration of Flexible DC Transmission, Hebei University of Technology, Tianjin 300401, PR China
[c] Ningbo Magnetic Materials Application Technology Innovation Center Co., Ltd., Ningbo, Zhejiang 315100, PR China

ARTICLE INFO

Keywords:
Soft magnetic composites
Soft magnetic ferrite
Powder metallurgy
Magnetic measurements
Power losses

ABSTRACT

Soft magnetic composites (SMCs) comprising an insulation coating and a soft magnetic powder matrix have the potential to extend the application frequency range of electromagnetic equipment and improve energy conversion efficiency. Producing high-performance SMCs in less time and low cost is highly demanded by industry and research. In this paper, a novel low-pressure spark plasma sintering (SPS) technique is designed to prepare SMCs, which have superior magnetic properties than those prepared by high-pressure methods. High-resistivity Ni-Zn ferrite is used to coat the pure iron powder matrix, and four SMCs with varying ferrite contents are prepared. Their structural characteristics of coating completeness are verified by SEM, and their mechanical, electrical, and magnetic properties are investigated comprehensively. A loss separation model for SMCs is established for evaluating the magnetic properties at high-frequency (20–200 kHz). The influences of the Ni-Zn ferrite content on the magnetic properties are compared based on experiments of various SMCs samples. The magnetic properties experiments indicates that the Ni–Zn ferrite contributed to the improvement of magnetic properties, including high permeability, saturation magnetization, and low remanence and coercivity. The study finds that 2.5 wt% Ni-Zn ferrite is the optimal percentage for producing pure iron powder matrix SMCs suitable for applications in the 20–200 kHz frequency range.

1. Introduction

As global energy issues intensify, emphasis on enhancing energy conversion efficiency and achieving sustainable development has grown increasingly significant. Power electronic devices are progressively evolving towards higher frequencies, miniaturization, and power capabilities [1–4]. Traditional soft magnetic materials cannot satisfy the energy conversion demands of these devices. Soft magnetic composites (SMCs), also known as magnetic powder cores, are soft magnetic materials formed by pressing soft magnetic powders coated with an insulating medium. Their overall performance is determined by the joint contributions of both the powder matrix and coating layers [5]. SMCs exhibit high saturation magnetic induction, permeability, and low core losses at high frequencies. Importantly, unlike traditional laminated materials, SMCs possess nearly isotropic magnetic properties in three dimensions, and specific-sized motor stators, rotors, and various magnetic cores can be manufactured directly using powder metallurgy technology [6].

As core losses at high frequencies are predominantly due to eddy current losses in the material, materials with high electrical resistivity should be used as coating materials to accommodate applications at higher frequencies. By perfectly encapsulating soft magnetic particles with an insulation layer, eddy currents are confined to individual particles and eddy current losses between particles are minimized [7]. Therefore, the selection of the powder matrix and coating material has a decisive influence on the performance of the SMCs. Unlike other organic or inorganic non-magnetic coatings, ferrite SMCs combine the advantages of both metallic soft magnetic materials and soft magnetic ferrites [8]. Using pure iron powder as the matrix for SMCs offers high saturation magnetic induction, high permeability, and low cost. However, pure iron has a relatively low electrical resistivity (approximately 10^{-6} Ω·cm), resulting in large core losses under high-frequency conditions, with an application frequency typically below 1000 Hz. In contrast, soft magnetic ferrites, with their higher electrical resistivity (10^3-10^7 Ω·cm), which is 10^7–10^{14} times that of common metallic soft magnetic materials, exhibit good high-frequency characteristics [9]. Among these,

* Corresponding author at: State Key Laboratory of Reliability and Intelligence of Electrical Equipment, Hebei University of Technology, Tianjin 300401, PR China.
E-mail address: jacklin7310@hotmail.com (Z. Lin).

https://doi.org/10.1016/j.jallcom.2024.178436
Received 23 October 2024; Received in revised form 28 December 2024; Accepted 31 December 2024
Available online 1 January 2025
0925-8388/© 2025 Elsevier B.V. All rights are reserved, including those for text and data mining, AI training, and similar technologies.

Ni-Zn ferrites can operate at frequencies as high as 1–500 MHz.

In ferrites, the magnetic moments in one sublattice are aligned opposite to those in another, partially canceling each other out and leading to lower spontaneous magnetization compared to other magnetic materials, such as pure iron. Nonetheless, compared to organic coatings, ferrite coatings enhance the overall saturation magnetic induction and permeability of the material and significantly extend the frequency range of applications for soft magnetic materials [10]. Furthermore, the Ni-Zn ferrite coating for SMCs, with a higher electrical resistivity than Mn-Zn ferrites [11], satisfies the requirements for high-frequency applications.

The properties of SMCs are significantly affected by the processing method used. How to form a uniform and complete coating layer has always been a focus of research. Currently, several processing methods are available for fabricating Ni-Zn ferrite coated SMCs. Peng et al. [12] employed a chemical co-precipitation method to prepare Ni-Zn ferrite coating on the surface of FeSi powders. However, the chemical co-precipitation method is complex and inevitably introduces organic solvents. Residual solvents can deteriorate the overall performance of the materials. In contrast, high-energy ball milling [13], a method known for its simplicity and rapid coating formation, mechanically attaches the coating particles to the substrate surface without mixing any non-magnetic substances. Sunday et al. [14] utilized a novel ultrasonic mixing technique to reduce milling time and achieve a more uniform coating layer.

The production of SMC samples utilizes powder metallurgy, an eco-friendly technology that helps reduce the manufacturing costs. SMCs can be molded into various shapes and sizes, allowing the customization of components to meet specific design requirements without wasting material [15]. The choice of compaction methods can affect the density of the material and the integrity of the insulating coating, which in turn influences the mechanical, electrical, and magnetic properties of the material. One feasible method is spark plasma sintering (SPS) [16], which facilitates rapid and dense particle bonding through electric sparks between particles, requires lower processing temperatures and shorter times, and does not require any binders, thereby significantly reducing the time and economic costs. Füzer et al. [17] employed boron-modified phenolic resin as a binder, achieving a maximum material density of only 6.72 g/cm^3 under a pressure of 600 MPa. In contrast, SPS can achieve densities close to the theoretical values without applying excessive pressure to the powders, thereby preventing damage to the coating layer and deterioration of material properties. This low-pressure and short-term high-quality sintering technology is required to achieve large-scale production of materials. In this paper, a low pressure (40 MPa) was used, and to our knowledge, few papers have previously studied such a low pressure. Cotojman et al. [18] sintered Mn-Zn ferrite SMCs using SPS and demonstrated that sintering at lower temperatures and shorter holding times did not alter the phase of the coating material, allowing for the formation of an intact coating while maintaining the ferrite's excellent magnetic and electrical properties. Commercial iron powder cores are typically pressed by cold pressing with an adhesive, resulting in lower iron losses below 3000 Hz. The SMCs produced by the method described in this paper have better loss characteristics at higher frequency (20–200 kHz) than commercial iron powder cores, significantly expanding the frequency range of electromagnetic device applications.

The goal of industrial production has always been to produce high-performance materials with simpler processes, shorter times, and less consumption, which is also the focus of this paper. In this paper, a cost-effective high-energy ball-milling method was employed to prepare SMC particles with varying percentages of Ni-Zn ferrite coatings on the pure iron powder matrix. Subsequently, SPS was used to sinter SMC powders into high-density samples with excellent magnetic properties. The structural, magnetic, and electrical properties of the materials were investigated. Finally, a high-frequency loss separation model was established, with an emphasis on investigating the mechanisms that affect the high-frequency iron losses of SMCs.

2. Experimental methods

Pure iron powders were mixed with Ni-Zn ferrites at 1 wt%, 2.5 wt%, 5 wt%, and 7.5 wt%, and the resulting mixtures were placed in an agate ball milling jar. The mixtures were subjected to high-energy planetary ball milling for 2 h without the addition of any organic solvent, at a milling speed of 500 rpm and a pause every 5 min. Subsequently, the powders were sintered using custom-designed SPS apparatus. The powders were added to a mold, pre-pressed, and then heated to 670°C at a pressure of 40 MPa for 5 min, with a subsequent holding time of 10 min. The entire process was conducted under vacuum, with the temperature precisely controlled using a thermocouple embedded in the mold[19].

The sintered samples, in the form of rings with an inner diameter of 20 mm, outer diameter of 30 mm, and height of 5 mm, were analyzed using X-ray diffraction (XRD, Smart Lab SE, Rigaku) for phase identification. Their microstructures were observed and analyzed using scanning electron microscopy (SEM, JSM-6510A, JEOL) along with energy-dispersive X-ray spectroscopy (EDS). The alternating current B-H curves of the samples were measured using a laboratory-built alternating current measurement platform, whereas the quasi-static B-H curves were measured using a vibrating sample magnetometer (VSM, Lakeshore 7407). The resistivity of the samples was determined using the four-point probe method [20]. All the measurements were conducted at room temperature.

3. Results and discussion

3.1. Characterization of sintered sample structure

Using the XRD patterns, it can be determined whether there is a significant phase transition in the main components of the powders before and after sintering. Fig. 1. displays the XRD spectrum of the Ni-Zn ferrite and mixed powders after ball milling. The diffraction peaks indicate that the ferrite exhibits a single-phase spinel cubic structure [21]. After ball milling, all peaks of Fe can be clearly observed in the spectrum of the mixed powders, but only partial peaks of Ni- Zn ferrite can be observed. Figs. 2(a) and 2(b) show the SEM images of the iron and Ni-Zn ferrite particles, respectively, before milling. The iron particles are irregularly ellipsoidal, while the Ni-Zn ferrite particles are irregularly fragmented and significantly smaller in diameter than the iron particles, which reduces the difficulty of mechanically attaching Ni-Zn ferrite to the iron particles.

Fig. 3 presents the SEM images of the four types of SMC powders after milling. In Fig. 3(a), the majority of the SMC powders still exhibit the characteristic grooves of the iron particle surfaces. However, as the ferrite content increases, the particle surfaces are gradually covered more completely, as shown in Fig. 3(b). With a further increase in the ferrite content, the surface of the powders becomes rougher, with numerous fine ferrite particles, as shown in Figs. 3(c) and 3(d). The XRD spectrums of the sintered samples with varying Ni-Zn ferrite content are shown in Fig. 4. Because of the minimal amount of Ni-Zn ferrite added, the primary component of the samples is Fe, and the XRD patterns prominently feature diffraction peaks at 44.8°, 65.1°, and 82.5°, corresponding to the (110), (200), and (211) crystal planes of α-Fe, respectively.

In the enlarged XRD spectrum, the peaks of Ni-Zn ferrite can be clearly observed at 29°, 36°, 57°, and 61°, which correspond to the (220), (311), (511), and (440) crystal planes, respectively. The mixing of different materials may lead to local stress changes in the crystal lattice, particularly the significant difference in grain size between Ni-Zn ferrite and Fe, which may generate compressive or tensile lattice dislocations, thereby affecting the position and half-width of the diffraction peaks. Moreover, owing to the inevitable introduction of stress during sintering

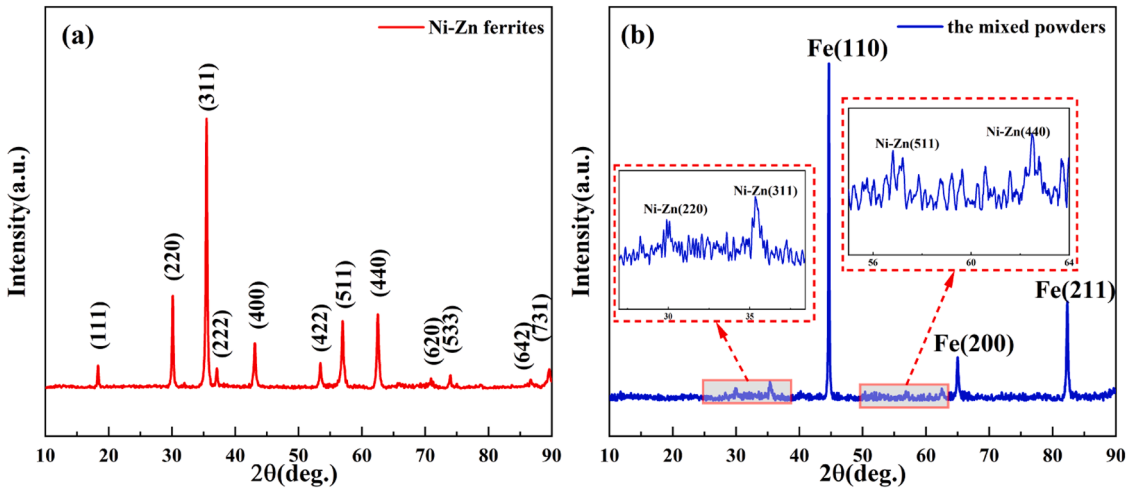


Fig. 1. XRD spectrum of (a)Ni-Zn ferrite (b)mixed powders after ball milling.

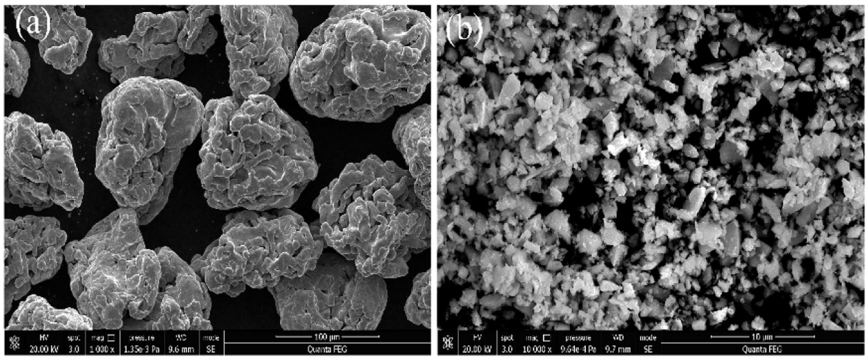


Fig. 2. (a) Pure iron particles and (b) Ni-Zn ferrite particles.

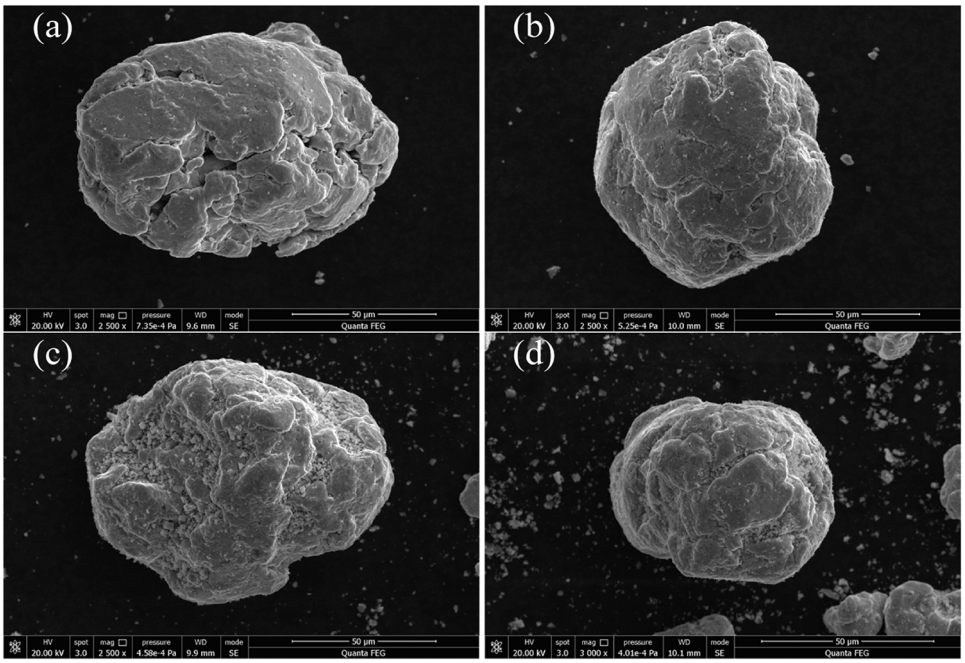


Fig. 3. SMC powders with ferrite content of (a) 1 wt% (b) 2.5 wt% (c) 5 wt% (d) 7.5 wt% after ball milling.

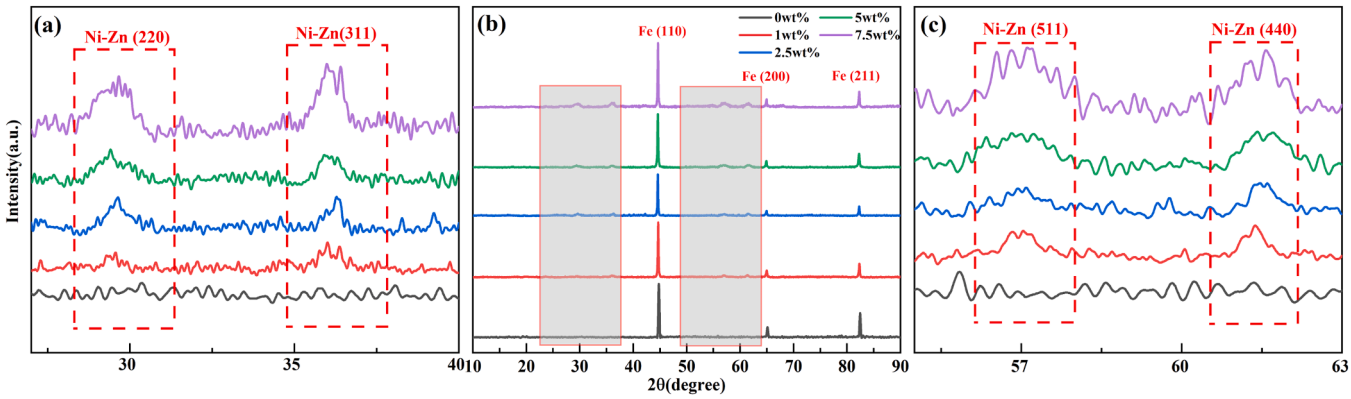


Fig. 4. (b) XRD images of samples with different Ni-Zn ferrite contents, (a) and (c) are partial enlarged view of Ni-Zn ferrite phase.

and polishing, the diffraction peaks of Ni-Zn ferrite are slightly shifted, as shown in Fig. 4(a) and (c). The intensities of these peaks increase with increasing Ni-Zn ferrite content. Consequently, the SPS process of SMCs does not obviously alter the phase composition of the original materials; thus, the high permeability and saturation magnetic induction properties of the iron particles are both inherited by the SMCs, as well as the high-frequency performance of Ni-Zn ferrite with low eddy current losses.

To evaluate the coating effect of the material, surface scanning and EDS analyses were performed on ring samples pressed with the four types of SMC powders. From the SEM and EDS results in Fig. 5, it can be inferred that the regions enriched in Ni, Zn, and O correspond to the Ni-Zn ferrite coating layer, which appears as darker areas in the SEM images. In Fig. 5(a), the EDS results show low visibility of Ni and Zn because of the insufficient thickness of the ferrite coating layer, which leads to more contact between the iron particles and the formation of multiple conductive pathways that affect the high-frequency performance of SMCs. As the ferrite content increases, the coating layer become more complete and its thickness increases. In Fig. 5(d), the Fe content decreases at the edges of the larger iron particles, while Ni, Zn, and O become concentrated at the edges, indicating that a sufficiently thick and complete ferrite coating layer is formed when the ferrite content reaches 7.5 wt%.

3.2. Physical characteristics

After ball-milling the mixture of pure iron and Ni-Zn ferrite, smaller ferrite particles adhere to the surfaces of the larger iron particles. As shown in Fig. 6, with an increase in the coating content, both the density and the filler factor of the samples initially increase and then decrease. The density and filler factor of the sample with 1 wt% ferrite are lower than those of the sample with 2.5 wt% ferrite. This discrepancy is due to the limited deformation of larger iron particles during the SPS process, which is insufficient to fill the pores between the particles. Additionally, the low ferrite content in the 1 wt% sample, as shown in Fig. 3(a), cannot effectively fill the pores between the iron particles. As the ferrite content increases, the pores between the iron particles are progressively filled, and the ferrite coating on the iron particles become thicker, thereby reducing the internal demagnetization fields. However, because the average density of ferrite (4.85 g/cm^3) is lower than that of iron (7.86 g/cm^3), excessive addition of brittle and hard ferrite can decrease the density of the sample and generate new pores, which in turn reduces the filler factor. An increase in these pores diminishes the mechanical strength of the sample, making it more susceptible to crack propagation and device failure during use [22]. Therefore, it can be preliminarily concluded that the optimal ferrite content to achieve the best mechanical performance of the sample is 2.5 wt%.

3.3. Magnetic and electrical characteristics

To evaluate the magnetic properties of the materials, we conducted VSM measurements, and the results are shown in Fig. 7. As the Ni-Zn ferrite content increases from 1 wt% to 7.5 wt%, the saturation magnetization of the SMCs decreases from 2.04 to 1.62 T. It can be explained by the increasing content of Ni-Zn ferrite with ferromagnetism in the SMCs which leads to a decrease in the overall magnetic properties.

In addition to being affected by the properties of the powder matrix and coating material, the magnetic properties of SMCs are also influenced by numerous factors. The pressure applied to the material during preparation is crucial. An appropriate pressure can produce high-density SMCs, thereby reducing the number of pores between particles and promoting tighter contact between particles, which is beneficial for magnetic circuit connectivity. Excessive pressure can introduce more magnetic domain pinning, making it more difficult for the domain wall to move during magnetization. In addition, it may cause damage to the insulation coatings, making it difficult to effectively suppress the eddy currents between particles. However, excessively low pressure will cause the material density to be too low to meet the requirements of practical applications and can even be unable to form.

Table 1 lists the relevant properties of previously published SMCs. It is evident that the pressure used in the SMCs in this paper is less than 1/10 that of similar SMCs, yet its density is still higher than that of most SMCs listed in Table 1, which makes the effective permeability of SMCs in this paper greater than that of the vast majority of SMCs [25]. This is because SPS can achieve low-pressure and high-density productions. Additionally, the saturation magnetization of SMCs with 1–7.5 wt% ferrite content is significantly higher than that of inorganic non-ferrite-coated materials prepared by Hao et al. [1]. Compared with the SMCs prepared by Tian et al. [2] using Mn-Zn ferrite coating, our SMCs with Ni-Zn ferrite show a slight improvement in magnetic properties. Compared with Ni-Zn ferrite coated SMCs sintered by SPS, the saturation magnetic flux density (1.62–2.04 T) of the SMCs in this paper is higher than that of the Fe powder matrix SMCs (1.65 T) [19] and FeSi powder matrix SMCs (1.52 T) [23], and the SMCs in this paper also show higher effective permeability than those SMCs. This proves that the SPS method with low pressure is helpful for improving the magnetic properties of SMCs.

The alternating magnetic properties of the ring SMC samples with wound coils were tested at various frequencies (50 Hz-200 kHz), as shown in Fig. 8. The test results at 50 Hz (Fig. 9 and Table 2) indicate that as the ferrite content increases, the coercivity and remanence of SMCs first increase and then decrease, and the permeability also exhibits a declining trend. When the ferrite content is changed from 2.5 wt% to 5 wt%, there are significant changes in the permeability, coercivity, and remanence of the materials. The decrease in permeability with increasing ferrite content is attributed to the lower permeability of

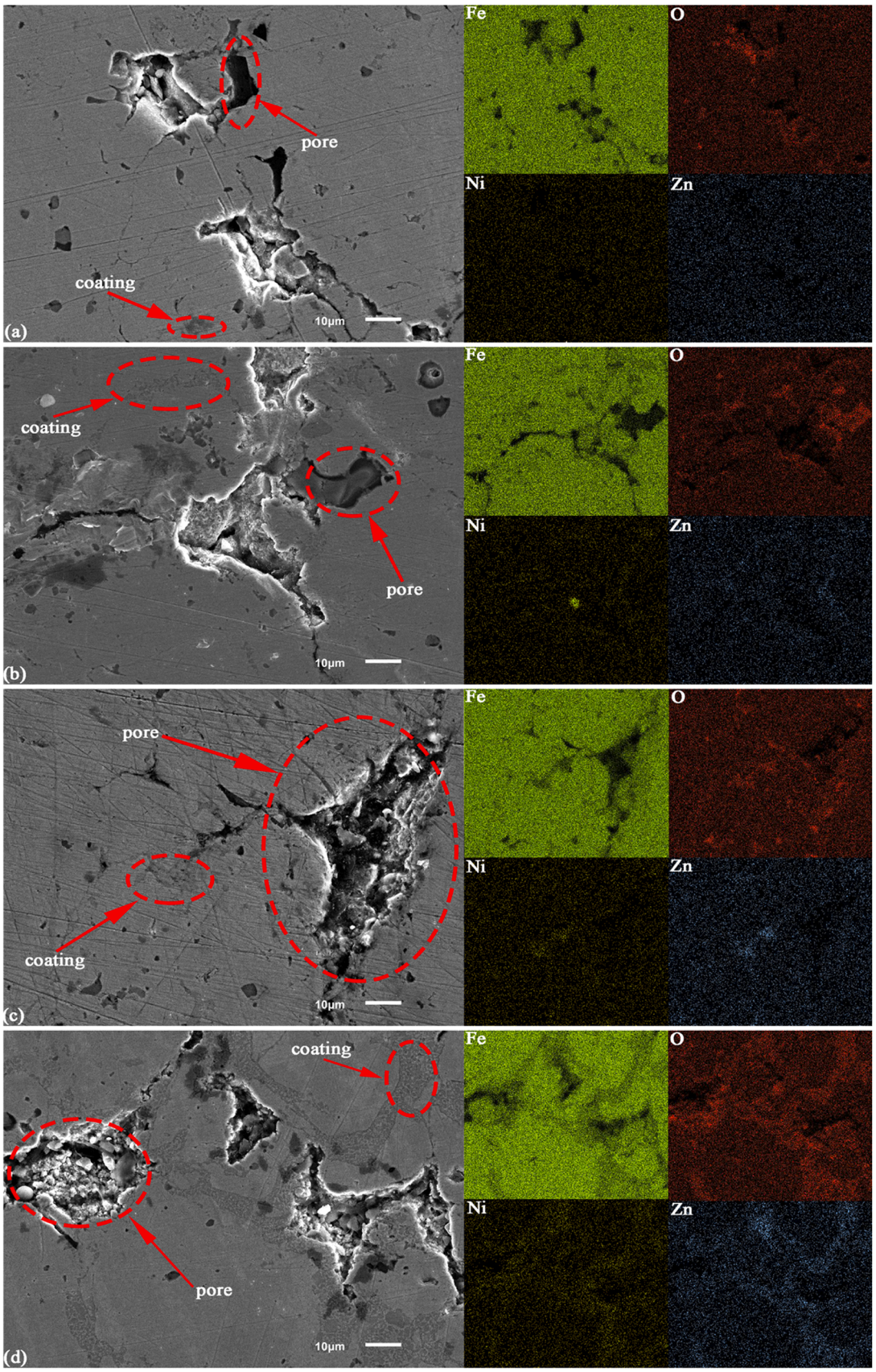


Fig. 5. SEM images and EDS elemental distribution maps of samples with (a) 1 wt%, (b) 2.5 wt%, (c) 5 wt%, and (d) 7.5 wt% Ni-Zn ferrite content.

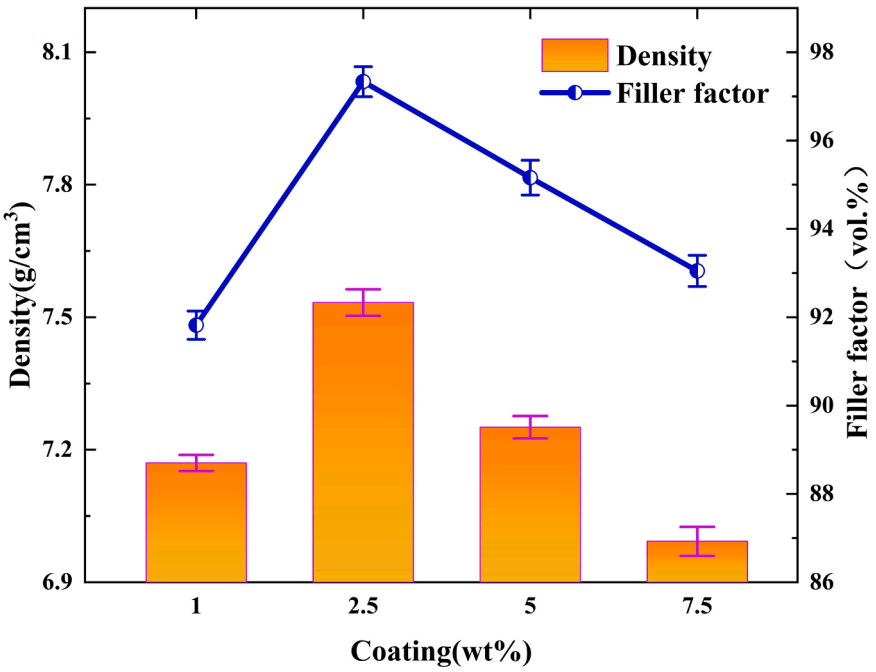


Fig. 6. Density and filler factor of samples with different coating contents. Error bars represent the maximum and minimum values of the samples.

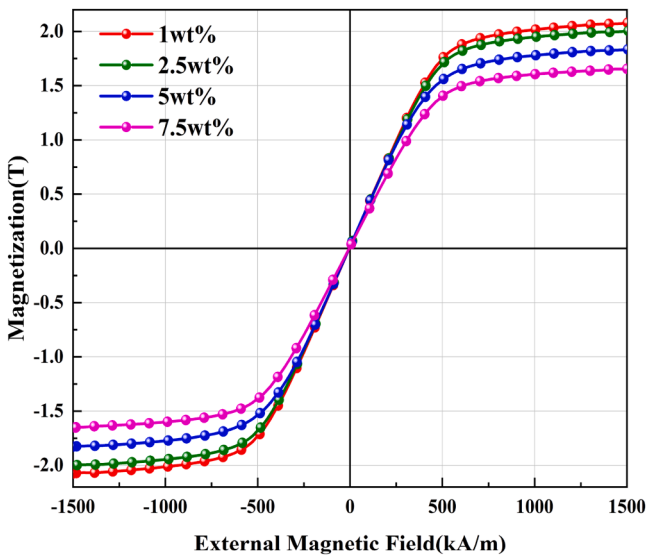


Fig. 7. VSM B-H curves of samples with different coating contents.

ferrite than that of iron. An increased amount of ferrite hinders the formation of a continuous magnetic circuit between iron particles as the thickness of the coating layer increases, leading to a higher proportion of low-magnetic ferrite in the magnetic circuit, which results in a reduction in the magnetic performance of the material.

The B-H curves of the 1 wt% and 2.5 wt% ferrite content samples exhibit no significant differences, as the ferrite content in the 1 wt% sample is insufficient to fill the pores between the iron particles. The additional ferrite primarily fills the remaining pores and completes the coating layer without significantly increasing its thickness or exacerbating the deterioration of the overall magnetic performance of the sample. The increase in sample resistivity with higher ferrite content is due to the significantly higher resistivity of ferrite compared to that of the iron powder matrix. Thus, the incorporation of more high-resistivity ferrite particles inevitably increases the overall resistivity of the sample.

3.4. Loss characteristics

Core loss is a crucial parameter at high frequencies, particularly when evaluating the performance of magnetic powder cores in practical applications. In an alternating magnetic field, core losses (P_{tot}) comprise hysteresis losses (P_h), eddy current losses (P_e), and excess losses (P_{exc}) [26]. Hysteresis losses refer to the work done during the magnetization due to the movement of magnetic domains against the internal friction

Table 1
Properties of state-of-the-art SMCs prepared by different methods.

SMCs	Pressure (MPa)	Temperature (℃)	Saturation magnetization M_s (emu/g)	Average efficient permeability μ_e	Average density (g/cm^3)
Iron @ Ni-Zn ferrite (this work)	40	670	188.7–233.1	235.1	7.18
FeSi @ Ni-Zn ferrite (SPS) [23]	600	520	-	131.8	-
Fe @ Ni-Zn ferrite (SPS) [19]	600	600	-	-	-
FeSi @ Ni-Zn ferrite [4]	2100	room temperature	-	-	6.74
Iron @ NiZnCu ferrite [14]	800	700	170.2–209.1	190.5	7.31
FeSi @ Mn-Zn ferrite [2]	1500	room temperature	198.9–205.5	150.9	6.73
FeSi @ $CaCO_3$ [1]	1600	room temperature	181.7–190.7	41.3	-
FeSiAl @ passivation agent [24]	1800	room temperature	145.1–150.2	80.3	-

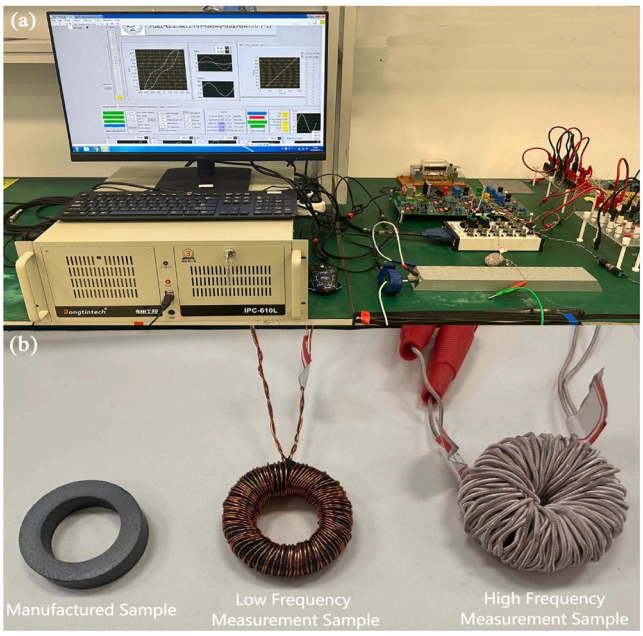


Fig. 8. (a)Alternating current measurement platform (b)SMC samples and AC test samples with wound coils.

within a magnetic material. Eddy current losses are caused by eddy currents owing to an alternating magnetic field. In SMCs, eddy current losses are divided into inter-particle eddy current losses (P_e^{inter}) and intra-particle eddy current losses (P_e^{intra}). P_e^{intra} primarily arises from eddy currents flowing within individual iron particles, whereas P_e^{inter} occurs when eddy currents flow along conductive paths between particles owing to incomplete insulation layers. Excess losses are often attributed to complex interactions between the magnetic domain structures, mainly caused by abnormal eddy current losses around the domain walls owing to the magnetic domain inhomogeneity [27]. Specifically, they arise owing to the evolution of domain walls that do not fully account for hysteresis and eddy-current losses. [28]. Fig. 10 shows the core losses of the samples with different ferrite contents at 20–200 kHz and 10mT. As the ferrite content increases, the core losses show a trend of first decreasing and then increasing, with the 2.5 wt% sample exhibiting the lowest core losses. We use the following empirical formula to separate the P_{tot}:

$$P_{tot} = P_h + P_e + P_{exc}$$

$$= K_h B_m^2 f + K_e B_m^2 f^2 + K_{exc} B_m^{1.5} f^{1.5} \quad (1)$$

where K_h, K_e, and K_{exc} are coefficients, B_m represents the magnetic flux density, and f denotes the frequency. By separating the P_{tot}, Fig. 11 is obtained. The fitting coefficients and errors for each component are listed in Table 3.

From Fig. 11(a), it can be observed that the hysteresis losses decrease

Table 2
Magnetic and electrical properties of SMC samples.

Ferrite content	Resistivity (mΩ·m)	Maximum permeability at 50 Hz	Coercive field at 50 Hz,1 T (A/m)	Remanence at 50 Hz,1 T (T)
1 wt%	0.400 ± 0.01	541 ± 5	809 ± 6	0.86 ± 0.05
2.5 wt%	0.447 ± 0.02	535 ± 5	827 ± 5	0.88 ± 0.01
5 wt%	0.518 ± 0.02	276 ± 2	1809 ± 10	0.59 ± 0.02
7.5 wt%	0.730 ± 0.02	179 ± 1	1156 ± 8	0.31 ± 0.01

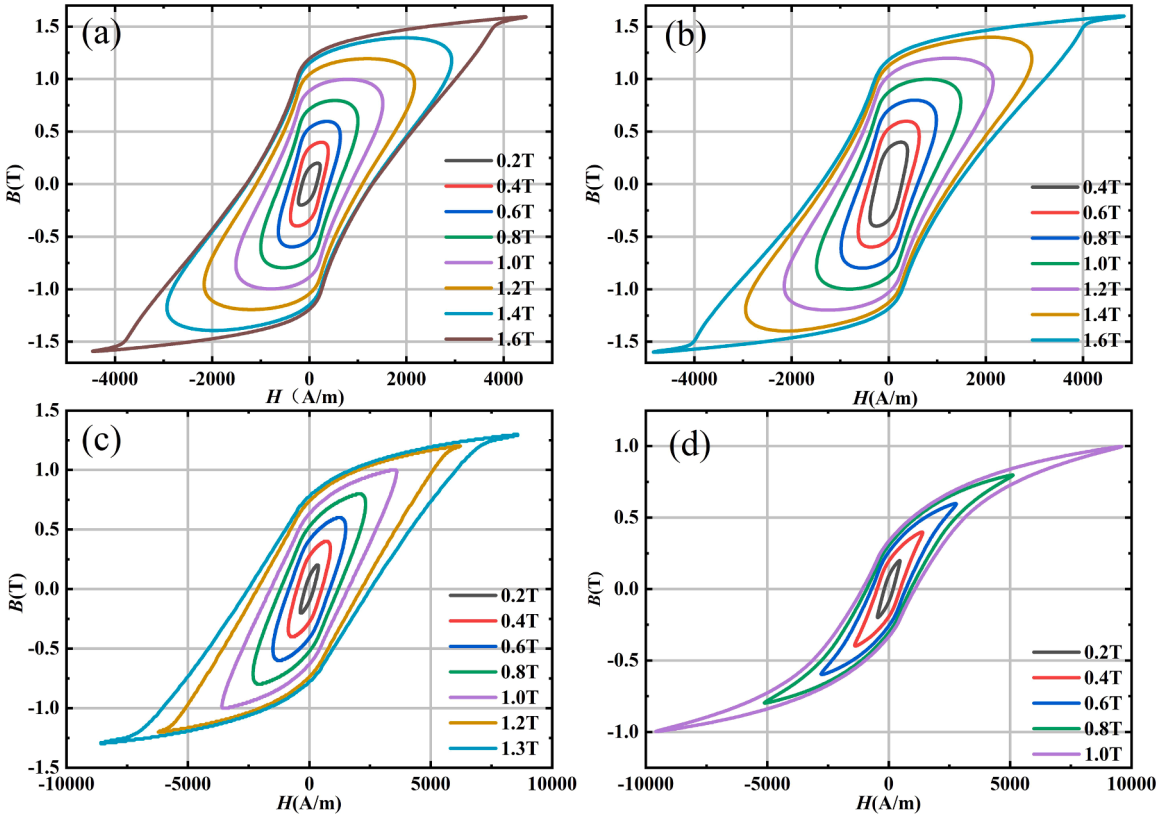


Fig. 9. B-H curves of samples with (a) 1 wt%, (b) 2.5 wt%, (c) 5 wt%, and (d) 7.5 wt% Ni-Zn ferrite content at 50 Hz.

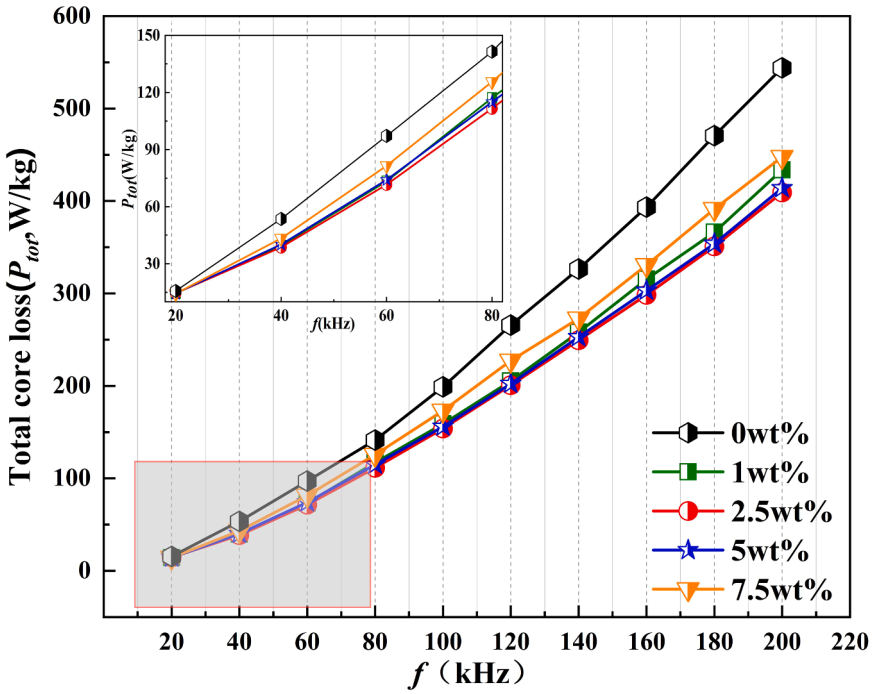


Fig. 10. Average core losses of samples with different ferrite contents at 20–200 kHz and 10mT.

with increasing ferrite content. It is attributed to the fact that a lower ferrite content cannot adequately fill pores. However, during the SPS process, pressure and temperature cause the iron particles to deform plastically, which helps fill some of the pores between the iron particles. This deformation introduces additional stress and pinning, which increase the hysteresis losses during the motion of the domain walls. Fig. 11(b) shows that the eddy current losses decrease with increasing ferrite content. The eddy current losses are decomposed into two components as follows:

$$P_e = P_e^{inter} + P_e^{intra} = \left(K_e^{inter} + K_e^{intra} \right) B_m^2 f^2 \tag{2}$$

$$K_e^{inter} = \frac{\sigma_{SMC} \left(\pi d \right)^2}{\beta \rho_{SMC}}, \; K_e^{intra} = \frac{\sigma_{Fe} \left(\pi d_{Fe} \right)^2}{6 \rho_{Fe}} \tag{3}$$

$$\beta = \frac{6}{1 - 0.633 \frac{w}{h} \tanh \left(\frac{1.58h}{w} \right)} \tag{4}$$

where ρ_{SMC} and ρ_{Fe} denote the densities of the SMCs and pure iron, respectively, σ_{SMC} and σ_{Fe} represent their electrical conductivities, d_{Fe} is the average particle diameter of the iron powder, β is the shape parameter of the rectangular cross-section of the ring samples, w and h are the width and height of the cross-section, respectively, and d is the shorter side of the cross-section. For general laminated soft magnetic materials, inter-particle eddy currents are much larger than intra-particle eddy currents, so the latter usually be ignored. However, in SMCs, the inter-particle eddy currents flowing within the cross-section are confined within individual particles. As shown in Table 3, the inter-particle eddy current no longer dominates. According to Eqs. (3) and (4), when the shape of the sample is fixed, the eddy current losses are inversely proportional to the resistivity of the sample. As the ferrite content increases, the resistivity of the sample gradually increases (Table 2), resulting in a decrease in eddy current losses, as calculated using Eqs. (2) and (3). However, it is assumed that the insulation coating uniformly surrounds the iron particles. In practice, the macro-resistivity of SMCs is not the only parameter that indicates the eddy current, because ferrites that do not form effective insulation coatings are also pressed into the samples during the powder metallurgy. This increases the overall resistivity of the material but does not significantly contribute to the isolation of eddy currents between particles. Fig. 5 shows that as the ferrite content increases, the insulation coating layer becomes progressively complete and thicker, effectively reducing the eddy currents between the particles. This is the actual reason for the

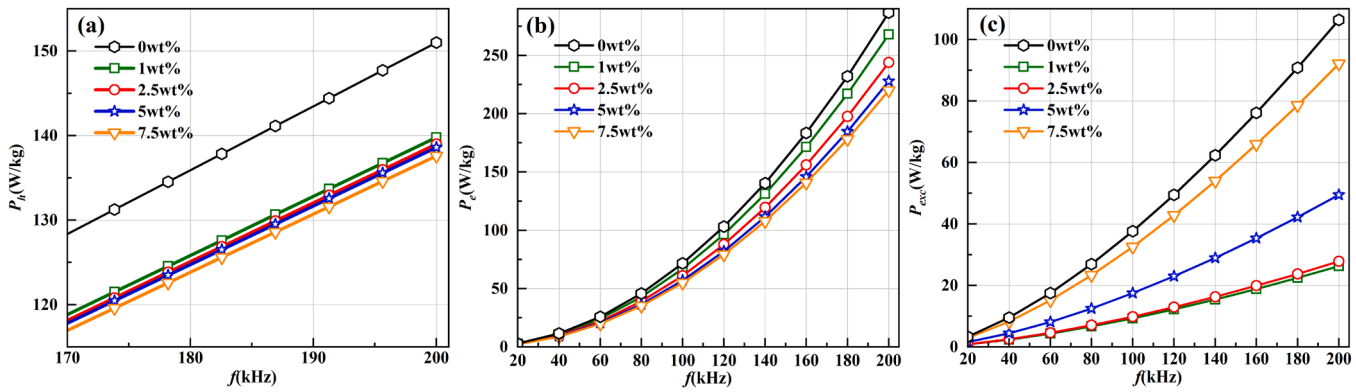


Fig. 11. (a) Hysteresis losses, (b) eddy current losses, and (c) excess losses of samples with different ferrite contents at 20–200 kHz, 10mT.

Table 3
Loss separation coefficients and calculation errors of SMCs with different ferrite contents.

Sample	K_h	K_e^{inter} $(\times 10^{-6})$	K_e^{intra} $(\times 10^{-5})$	K_{exc} $(\times 10^{-4})$	Average error of formula calculation
0 wt%	7.55	8.19	6.35	11.89	8.19 %
1 wt%	7.00	4.54	6.23	2.94	6.28 %
2.5 wt%	6.96	3.67	5.69	3.11	6.64 %
5 wt%	6.94	4.69	5.22	5.35	6.75 %
7.5 wt%	6.89	3.75	5.08	10.26	8.50 %

decrease in eddy current losses with increasing ferrite content.

Excess losses are often neglected at low frequencies, but become particularly significant under high-frequency magnetic fields. Although the exact mechanism of excess losses is not yet clear, Bertorri's theory [29] suggests that excess losses typically occur around the movement of domain walls and are related to the difficulty of domain motion. In addition, the strength and flow path of the eddy current may influence the local effective field, causing abnormal motion of the domain walls, which can affect excess losses. Therefore, excess losses are also affected by the combined effects of intra-particle eddy currents and inter-particle eddy currents in SMCs. The magnitude of excess losses can be characterized by the number of active magnetic objects (AMOs) in the material. The mean of the AMOs in the sample (n) is determined by the sum of all the fields (H_w) during magnetization and the excess magnetic field (H_{exc}) acting on the domain walls:

$$n = \frac{H_w}{H_{exc}} \tag{5}$$

$$H_w = \frac{4GSB_m f}{\rho_{Fe}} \tag{6}$$

$$H_{exc} = H_d - H_c = \frac{P_{exc}}{4B_m f \rho_{SMC}} \tag{7}$$

where H_d and H_c represent the dynamic and static coercive fields, respectively, S is the area of the rectangular cross-section of the ring sample, and the dimensionless coefficient of eddy current damping G is typically set to 0.1356 [30]. The means of the AMOs in the different samples were calculated at 10 mT, 100 kHz, and 200 kHz, as detailed in Table 4.

From Fig. 11(c), it can be observed that at high frequencies, the excess losses increase significantly with ferrite content. This means that the higher the ferrite content, the more energy consumed by the magnetic domain movement of the SMCs during magnetization. Table 4 shows that the ferrite content is inversely proportional to the number of AMOs n in SMCs. Therefore, it can be concluded that the greater the number of AMOs, the less energy is required for magnetic domain movement, and the easier it is for magnetization to occur. From a microscopic perspective, the samples with higher ferrite content contain a higher proportion of small ferrite particles, which form more domain wall pinning on their surfaces. Meanwhile, more inter-particle pores lead to a larger local demagnetization field and weaker internal magnetic interactions, leading to a reduced number of AMOs. Thus, while the introduction of a higher ferrite content increases the resistivity of the sample and reduces eddy current losses, it also leads to a significant increase in excess losses. The sample with 2.5 wt% ferrite exhibits lower eddy current losses and excess losses, resulting in optimal performance within the frequency range of 20–200 kHz. As derived from Eq. (1), under higher frequency conditions, eddy current losses become dominant and increase at the fastest growth rate with frequency. Therefore, it is anticipated that the 7.5 wt% ferrite content sample with the lowest eddy current loss coefficient (K_e) will demonstrate the best performance in applications above megahertz.

Table 4
Average number of AMOs in four samples with different ferrite contents at 10mT, 100 kHz, and 200 kHz.

Sample	The mean of AMOs at 100kHz	The mean of AMOs at 200kHz
0 wt%	1.40	1.98
1 wt%	5.64	7.99
2.5 wt%	5.17	7.32
5 wt%	3.11	4.39
7.5 wt%	1.56	2.21

4. Conclusion

This paper analyzes the performance differences of SMCs made with four different contents of Ni-Zn ferrite using an SPS apparatus, demonstrating that the SPS apparatus can produce SMCs with excellent performance using very low pressure. It was found that under low-frequency (50 Hz) conditions, the sample with a coating content of 7.5 wt% exhibits superior soft magnetic properties, although its saturation magnetic induction and permeability are lower than those of the other samples.

At higher frequency (20–200 kHz), although a higher ferrite content is beneficial for reducing eddy current losses, it significantly increases excess losses. Within this frequency range, the core losses initially decrease and then increase with increasing coating content. The sample with a 2.5 wt% coating content shows the optimal loss characteristics in this frequency range, while also having a higher average density (7.54 g/cm^3) and the highest average filler factor (97.4 %). Thus, it is identified as the best ratio for producing SMCs in high-frequency power electronic devices.

Overall, this paper presents a comprehensive method for evaluating and optimizing core losses, permeability, and saturation magnetic induction in SMCs. Balancing this contradiction is essential for potential high-power and high-frequency applications of SMCs.

CRediT authorship contribution statement

Li Yongjian: Resources, Project administration, Funding acquisition, Conceptualization. **Zhang Changgeng:** Writing – review & editing, Resources, Project administration, Funding acquisition. **Lin Zhiwei:** Writing – review & editing, Supervision, Resources, Project administration, Methodology, Formal analysis, Conceptualization. **Ziran Guo:** Writing – original draft, Validation, Methodology, Investigation, Data curation.

Declaration of Competing Interest

The authors declare that they have no known competing financial interests or personal relationships that could have appeared to influence the work reported in this paper.

Acknowledgements

This work was supported in part by the National Natural Science Foundation of China, (No. 52277008 , 92066206), and Natural Sciences funddation of Hebei Province, China (E2023202050) .

Data availability

The data that has been used is confidential.

References

[1] H. He, Y. Liu, Z. Cui, Z. Huang, Z. Wu, Q. Hou, High-performance Fe–6.5wt%Si/CaCO3 soft magnetic composites prepared via the thermal decomposition of calcium acetate, J. Phys. Chem. Solids 190 (2024) 112012.

[2] T. Yang, K. Lu, J. Wang, J. Xu, Z. Zheng, X. Liu, Fe-6.5 wt%Si soft magnetic composites with significant improvement of magnetic properties by compositing nano-MnZn ferrites, J. Alloy. Compd. 909 (2022) 164660.

[3] Z. Guo, J. Wang, W. Chen, D. Chen, H. Sun, Z. Xue, C. Wang, Crystal-like microstructural Finemet/FeSi compound powder core with excellent soft magnetic properties and its loss separation analysis, Mater. Des. 192 (2020) 108769.

[4] J. Wang, Z. Xue, S. Song, H. Sun, Magnetic properties and loss separation mechanism of FeSi soft magnetic composites with in situ NiZn-ferrite coating, J. Mater. Sci. Mater. Electron. 32 (2021) 20410–20421.

[5] M.C. Kulan, N.J. Baker, K.A. Liogas, O. Davis, J. Taylor, A.M. Korsunsky, Empirical Implementation of the Steinmetz Equation to Compute Eddy Current Loss in Soft Magnetic Composite Components, IEEE Access 10 (2022) 14610–14623.

[6] M. Ali, F. Ahmad, A review of processing techniques for Fe-Ni soft magnetic materials, Mater. Manuf. Process. 34 (2019) 1580–1604.

[7] K. Shi, D. Zhang, Z. Ren, D. Chen, Y. Zhang, C.-S. Koh, Effect of particles Size on Eddy-current loss of soft magnetic composites using combined DEM and FEM, IEEE Trans. Magn. 60 (2024) 1–8.

[8] Z. Birčáková, F. Onderko, S. Dobák, P. Kollár, J. Füzer, R. Bureš, M. Fáberová, B. Weidenfeller, J. Bednarčík, M. Jakubčin, J. Szabó, M. Dilyová, Eco-friendly soft magnetic composites of iron coated by sintered ferrite via mechanofusion, J. Magn. Magn. Mater. 543 (2022) 168627.

[9] L.-G. Petrescu, M.-C. Petrescu, V. Ioniță, E. Cazacu, C.-D. Constantinescu, Magnetic properties of manganese-zinc soft ferrite ceramic for high frequency applications, Materials 12 (2019) 3173.

[10] W. Burgess, J. Devkota, B. Howard, Wet chemistry-synthesized Fe/mixed ferrite soft magnetic composites for high-frequency power conversion, AIP Adv. 14 (2024) 025212.

[11] A.A. Sattar, H.M. El-Sayed, K.M. El-Shokrofy, M.M. El-Tabey, Effect of manganese substitution on the magnetic properties of nickel-zinc ferrite, J. Mater. Eng. Perform. 14 (2005) 99–103.

[12] Y. Peng, Y. Yi, L. Li, H. Ai, X. Wang, L. Chen, Fe-based soft magnetic composites coated with NiZn ferrite prepared by a co-precipitation method, J. Magn. Magn. Mater. 428 (2017) 148–153.

[13] K. Geng, Y. Xie, L. Yan, B. Yan, Fe-Si/ZrO2 composites with core-shell structure and excellent magnetic properties prepared by mechanical milling and spark plasma sintering, J. Alloy. Compd. 718 (2017) 53–62.

[14] K.J. Sunday, M.L. Taheri, NiZnCu-ferrite coated iron powder for soft magnetic composite applications, J. Magn. Magn. Mater. 463 (2018) 1–6.

[15] E.A. Périgo, B. Weidenfeller, P. Kollár, J. Füzer, Past, present, and future of soft magnetic composites, Appl. Phys. Rev. 5 (2018) 031301.

[16] S. Lu, M. Wang, Z. Zhao, Recent advances and future developments in Fe-based amorphous soft magnetic composites, J. Non Cryst. Solids 616 (2023) 122440.

[17] L. Dakova, J. Fuzer, S. Dobak, P. Kollar, Y. Osadchuk, M. Streckova, M. Faberova, R. Bures, P. Kurek, M. Vojtko, Analysis of magnetic losses and complex permeability in novel soft magnetic composite with ferrite nanofibers, IEEE Trans. Magn. 54 (2018) 1–6.

[18] L. Cotojman, T.F. Marinca, F. Popa, B.V. Neamțu, V.C. Pricǎ, I. Chicinaș, Producing soft magnetic composites by spark plasma sintering of pseudo core–shell Ni–Fe Alloy@Mn0.5Zn0.5Fe2O4 powders, Materials 16 (2023) 501.

[19] M. Wang, Z. Zan, N. Deng, Z. Zhao, Preparation of pure iron/Ni–Zn ferrite high strength soft magnetic composite by spark plasma sintering, J. Magn. Magn. Mater. 361 (2014) 166–169.

[20] S. Saberi, M. Stockinger, C. Stoeckl, B. Buchmayr, H. Weiss, R. Afsharnia, K. Hartl, A new development of four-point method to measure the electrical resistivity in situ during plastic deformation, Measurement 180 (2021) 109547.

[21] M. Kurian, D.S. Nair, Effect of preparation conditions on Nickel Zinc Ferrite nanoparticles: a comparison between sol–gel auto combustion and co-precipitation methods, J. Saudi Chem. Soc. 20 (2016) S517–S522.

[22] M. Yakout, M.A. Elbestawi, S.C. Veldhuis, Density and mechanical properties in selective laser melting of Invar 36 and stainless steel 316L, J. Mater. Process. Technol. 266 (2019) 397–420.

[23] Y. Zhou, M. Wang, Y. Chi, X. Qu, P. Liu, Z. Zhao, Preparation of Fe–6.5 wt% Si/Ni0.5 Zn0.5 Fe2 O4 Soft Magnetic Composite With Low Total Loss, IEEE Trans. Magn. 52 (2016) 1–4.

[24] S. Tong, Structure and magnetic properties of FeSiAl-based composites with the compound passivation agent, Phys. Scr. (2023).

[25] J. Wang, Improvement in core losses for FeSiAl soft magnetic composites induced by powder annealing treatment, J. Mater. Res. Technol. 24 (2023) 2500–2513.

[26] P. Kollár, Z. Birčáková, J. Füzer, R. Bureš, M. Fáberová, Power loss separation in Fe-based composite materials, J. Magn. Magn. Mater. 327 (2013) 146–150.

[27] Y. Gao, Y. Araki, H. Dozono, K. Muramatsu, W. Guan, J. Yuan, C. Tian, B. Chen, Modeling of anomalous Eddy current losses due to movement of domain walls in particles of a soft magnetic composite, IEEE Trans. Magn. 56 (2020).

[28] O. De La Barrière, C. Appino, F. Fiorillo, C. Ragusa, H.B. Ahmed, M. Gabsi, F. Mazaleyrat, M. LoBue, Loss separation in soft magnetic composites, J. Appl. Phys. 109 (2011) 07A317.

[29] G. Bertotti, General properties of power losses in soft ferromagnetic materials, IEEE Trans. Magn. 24 (1988) 621–630.

[30] A.P.S. Baghel, S.V. Kulkarni, Dynamic loss inclusion in the Jiles–Atherton (JA) hysteresis model using the original JA approach and the field separation approach, IEEE Trans. Magn. 50 (2014).